

Electronic Supplementary Information (ESI)

Insight into the phase evolution of NiMgAl catalyst from reduction to post-reaction for dry reforming of methane

Zhenghong Bao,^a Yiqiu Zhan,^a Jason Street,^b Wenqian Xu,^c Filip To,^a Fei Yu^{a,*}

^a Department of Agricultural and Biological Engineering, Mississippi State University, Mississippi State, MS 39762, USA

^b Department of Sustainable Bioproducts, Mississippi State University, Mississippi State, MS 39762, USA

^c X-ray Science Division, Advanced Photon Source, Argonne National Laboratory, Argonne, IL 60439, USA

* Corresponding author. Tel.: 6623250206. E-mail address: fyu@abe.msstate.edu (F. Yu).

Contents

Experimental	2
Catalyst preparation	2
H₂-TPR	2
<i>In situ</i> XRD	3
TEM	4
TGA	4
Table S1 (ascribe amorphous Al₂O₃)	5
Table S2 (ascribe NiO and MgO)	6
Table S3 (ascribe NiAl₂O₄ and MgAl₂O₄)	7
Fig. S1 (<i>in situ</i> XRD reactor)	8
Fig. S2 (Intensity of Ni and Spinel support)	9
Fig. S3 (TEM images)	10
Fig. S4 (TGA curve)	11
Fig. S5 (RGA results)	12
Fig. S6 (d-spacing & crystallite size on each reflection)	13
Fig. S7 (lattice parameter and unit cell volume at reduction and DRM reaction stages)	14
Fig. S8 (lattice parameter and unit cell volume at cooling stage)	15
Cal. S1 (Determining the composition of NiO_{free}, NiO_{int.} and NiAl₂O₄)	16
Cal. S2 (Determining the effect of temperature on the peak intensity)	17
Cal. S3 (Determining the reduction degree of NiAl₂O₄)	18
Cal. S4 (Determining the phase compositions of fresh and reduced catalysts)	19
Reference	20

Experimental

Catalyst preparation

A NiMgAl composite oxide catalyst was prepared using a refluxed co-precipitation method as described in our previous report¹ with some adjustments of preparation parameters. All chemicals were purchased from Sigma-Aldrich (St. Louis, MO) and used as received. Stoichiometric quantities of $\text{Ni}(\text{NO}_3)_2 \cdot 6\text{H}_2\text{O}$, $\text{Mg}(\text{NO}_3)_2 \cdot 6\text{H}_2\text{O}$ and $\text{Al}(\text{NO}_3)_3 \cdot 9\text{H}_2\text{O}$ were dissolved in distilled water to achieve a 0.2 M reagent solution. The resulting solution and an aqueous solution of sodium hydroxide (1 M) were dropped-wise into a Florence flask with a constant stirring rate of 600 RPM and pH value of 11 ± 0.05 at 40 °C. At the end of precipitation, the flask was heated to 100 °C to reflux the precipitate suspension using a graham condenser with continuous stirring for 24 hours. Thereafter, the refluxed suspension was thoroughly washed and filtrated with distilled water several times so that the filtrate had a final pH of 7. The resulting precipitate was dried at 110 °C for 12 h, and then grounded into fine powder and calcined at 850 °C for 4 h in air. The calcined oxide fresh catalyst contained metal elements of 11mol % Ni, 20mol % Mg, and 69 mol % Al, which is designated as NiMgAl.

H₂-TPR

The H₂ temperature programmed reduction (H₂-TPR) analysis of the calcined catalyst was carried out on a Quantachrome ChemBET Pulsar TPR/TPD apparatus (Quantachrome Instruments, Boynton Beach, FL) equipped with a thermal conductivity detector (TCD). Prior to the TPR experiment, ~30 mg fresh catalyst was loaded between two pieces of quartz wool at the bottom of a U type quartz micro-reactor and then purged with 70 mL/min N₂ gas at 300 °C for 1 h to remove the trace amount of water and other adsorbents and then cooled to 50 °C. The pre-treated catalyst was heated from 50 °C to 1000 °C (10 °C/min) in a 5% H₂/He mixture at a flow rate of 70 mL/min. The H₂ consumption during the reduction process was measured by analysing the effluent gas with TCD.

***In situ* XRD**

The *in situ* synchrotron X-ray powder diffraction experiment was performed using the beamline 17-BM ($\lambda = 0.72768\text{\AA}$) at the Advanced Photon Source at Argonne National Laboratory. A synchrotron X-ray beam with a diameter of 0.3 mm was used to irradiate the sample and a Perkin-Elmer flat panel area detector located at 200 mm downstream of the sample was applied to receive X-ray photons and then obtain XRD patterns. A lanthanum hexaboride (LaB_6) standard was used to calibrate the detector orientation. About 5 mg of the NiMgAl catalyst sample was loaded in the quartz capillary tube (i.d. = 0.7 mm) and sandwiched between two pieces of quartz wool. Two heating coils were installed immediately below and above the capillary reactor,^{2,3} and the temperature was monitored using a 0.5 mm type K thermocouple that was placed in the capillary next to the sample (Fig. S1). A residual gas analyser (RGA)⁴ was connected to the outlet of the reactor to monitor the component of tail gas using mass spectroscopy during the entire *in situ* XRD experiment.

The *in situ* XRD experiment was consisted of continuous data acquisition during the catalyst reduction, dry reforming of methane (DRM) reaction and post reaction stages. The capillary reactor was loaded with fresh catalyst and heated from room temperature to 850 °C using a ramping rate of 5 °C/min and hold for 2h at 850 °C in the reduction gas flow of 3.5% H_2/He (30 mL/min). Thereafter, the sample was cooled to 700 °C in the same gas flow in 5 min, then switched to the feed gas (5% CO_2 /5% CH_4/He) at a flow rate of 30 mL/min to perform the DRM reaction. The temperature was kept at 700 °C for 1 h, then increased to 750 °C in 30 min and kept for 1h, again raised to 800 °C in 30 min and kept for 1h. After the DRM reaction, the catalyst sample was controlled to cool to room temperature in 15 min. The diffraction data were continuously collected every other 50 s (10 s/scan, i.e. 1 scan/min) from the beginning of catalyst reduction to the final cooling to room temperature. It takes about 10 seconds to complete one scan of synchrotron XRD from 5 to 45° of the 2θ angle. Due to the celerity of data acquisition, the temperature was considered to be constant for each scan (0.83 °C rising in 10 s at 5 °C/min) during the temperature rising. The identification of phase structure was performed by comparing the experimental diffraction angle with the converted 2θ from ICDD card. The regular

diffraction angle of $2\theta_1$ (Cu K α , $\lambda_1=1.5406 \text{ \AA}$) from potential ICDD card was converted into $2\theta_2$ ($\lambda_2=0.72768\text{\AA}$) via the derivative equation of Bragg's law (Eq. 1).

$$\theta_2 = \arcsin\left(\frac{\lambda_2}{\lambda_1}\sin\theta_1\right) \quad \text{Eq.1}$$

TEM

Morphology of the used catalyst was observed with a JEOL JEM-2100 transmission electron microscope (TEM, Waterford, VA) operated at 200 kV. The catalyst sample was dispersed in ethanol and vibrated for 20 min in an ultrasonic bath to obtain a suspension, 3 drops of which was dropped onto a 300 mesh copper grid coated with a honey carbon film. The grid was then dried on a filter paper in a vacuum oven at 70 °C, followed by inspection with the TEM. The energy dispersive X-ray spectroscopy (EDS) mapping was performed in a STEM mode.

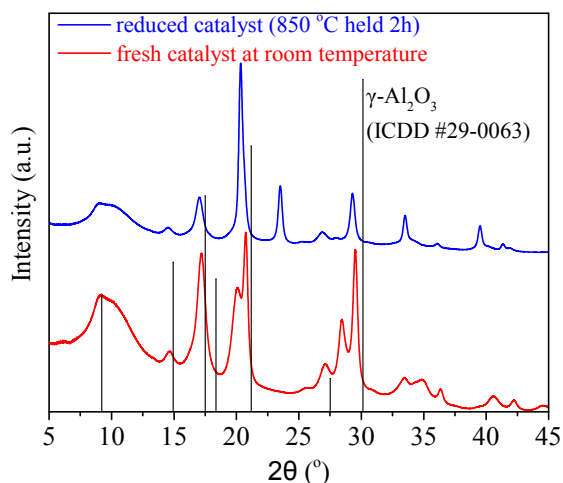
TGA

To confirm the carbon-free observation, the *in situ* XRD used sample was conducted a thermal gravimetric analysis (TGA) on an equipment of Shimadzu TGA-50 (Columbia, MD). About 2 mg of the *in situ* XRD used catalyst was heated with a ramping rate of 10 °C/min from room temperature to 1000 °C.

Table S1 (ascribe amorphous Al₂O₃)Table S1 Comparing the experimental observed 2θ with the transferred amorphous Al₂O₃

Fresh observed broad peak 2θ (°)	7	14	Reference
Amorphous Al ₂ O ₃	15	30	⁵
Transferred amorphous Al ₂ O ₃	7.07	14.04	Eq.1 in this work

In addition:

Fig. S0 The comparison of observed diffraction angles and converted 2θ from ICDD #29-0063 card.

It was reported⁵ that the regular diffraction angle of an amorphous Al₂O₃ phase ranges from 15 to 30°, which can be converted to the synchrotron diffraction angle of 7.07-14.04°, which is consistent with the experimental observation of 7-14°. Therefore, the aluminum oxide in the NiMgAl catalyst is amorphous Al₂O₃.

In addition, the γ -Al₂O₃ standard diffraction angles (ICDD #29-0063) were selected and converted to compare with the observed 2θ (Fig. S0). Because the γ -Al₂O₃ phase could be acquired when the mixed phase aluminum oxide was thermally treated at 600-875 °C,⁶ and here the NiMgAl catalyst was calcinated at 850 °C. From Fig. S0, we can easily conclude that there was no γ -Al₂O₃ in either fresh or reduced NiMgAl catalyst. Therefore, both direct and indirect proofs show that the aluminum oxide in NiMgAl catalyst should be amorphous Al₂O₃.

Table S2 (ascribe NiO and MgO)

Table S2 Comparison of the experimental observed 2θ and the transferred ICDD card for the NiO and MgO phases.

Fresh observed 2θ (°)	17.23	20.09	28.45	33.46	34.92	40.57
NiO (ICDD# 47-1049)	17.35	20.06	28.52	33.57	35.12	40.78
MgO (ICDD# 04-0829)	17.21	19.90	28.29	33.29	34.82	40.41
Distance to NiO (%)	0.70	0.15	0.24	0.34	0.56	0.52
Distance to MgO(%)	0.09	0.96	0.58	0.49	0.29	0.38
NiO intensity	61	100	35	13	8	4
MgO intensity	10	100	52	4	12	5
NiO and MgO reflection	(111)	(200)	(220)	(311)	(222)	(400)

The smaller the distance between the observed 2θ and the transferred ICDD 2θ , the better a match is acknowledged. From Table S2, we can see that the observed 2θ had a better match with NiO phase than the MgO phase, although both of them are very similar. This indicates that NiO phase contribute to the observational 2θ more than the MgO phase. But we could not eliminate the existence of MgO phase in the fresh sample that was calcined at 850 °C, because the monolithic magnesia-alumina spinel requires a calcination temperature of 1300 °C.⁷

Table S3 (ascribe NiAl₂O₄ and MgAl₂O₄)

Table S3 Comparison of the experimental observed 2θ and the transferred ICDD card for the NiAl₂O₄ and MgAl₂O₄ spinel structure.

Fresh observed 2θ (°)	9.07	14.67	17.23	20.75	27.12	29.51	36.35
Reduced 2θ (°)	9.01	14.54	17.04	20.34	27.05	29.30	36.10
NiAl ₂ O ₄ (ICDD# 10-0339)	8.98	14.69	17.24	20.83	27.18	29.62	36.52
MgAl ₂ O ₄ (ICDD# 21-1152)	8.96	14.63	17.17	20.75	27.06	29.50	36.34
NiAl ₂ O ₄ intensity	20	20	100	65	30	60	8
MgAl ₂ O ₄ intensity	35	40	100	65	45	55	6
NiAl ₂ O ₄ & MgAl ₂ O ₄ index	(111)	(220)	(311)	(400)	(511)	(440)	(444)

Table S3 shows that the nickel aluminate (ICDD# 10-0339) had a higher 2θ value than that of the magnesium aluminate (ICDD# 21-1152) at each position. Most of the fresh observed 2θ located between the 2θ of these two spinel structures indicates that the fresh catalyst contained both NiAl₂O₄ and MgAl₂O₄.

After the entire reduction process, the observed 2θ decreased away from the standard diffraction angle of NiAl₂O₄ but came close to that of MgAl₂O₄, suggesting the reduction of nickel aluminate.

We postulate that the MgAl₂O₄ phase neither formed from the MgO and Al₂O₃ phases nor decompose to them at the reduction temperature of 850 °C, because the fresh sample had been calcinated at 850 °C for 4 h. The possible formation/decomposition of the magnesium aluminate has already been completed during the catalyst calcination.

Fig. S1 (*in situ* XRD reactor)

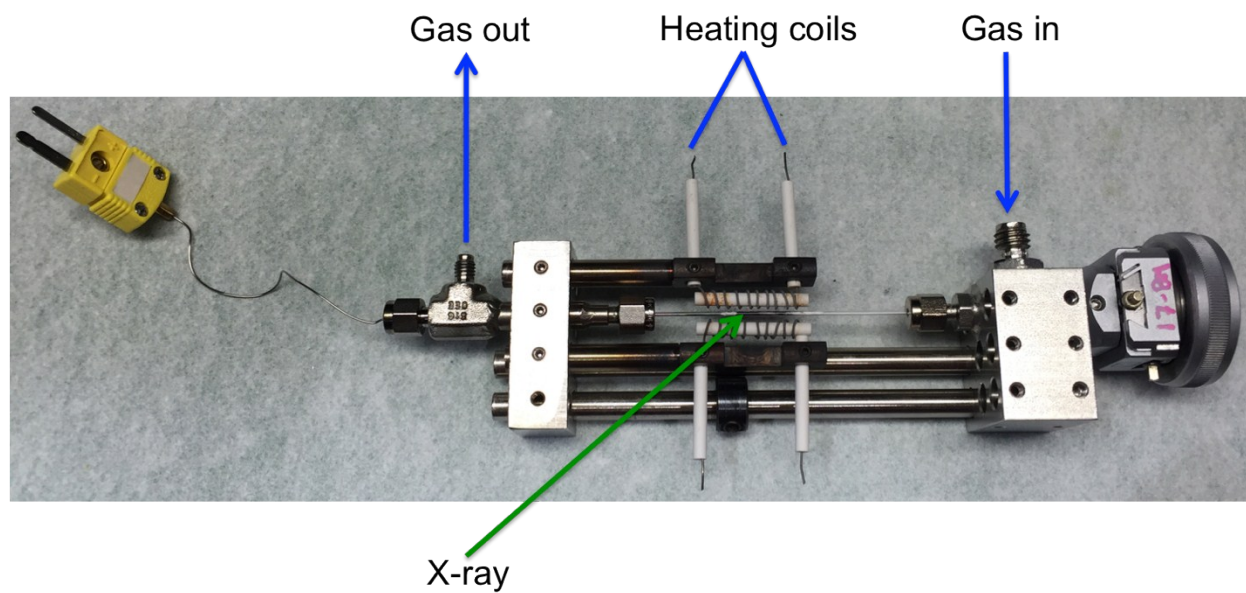


Fig. S1 The quartz capillary reactor used for *in situ* XRD measurement at 17-BM. More details about this quartz capillary reactor can be referred in the literature reported by Chupas et al.⁸

Fig. S2 (Intensity of Ni and Spinel support)

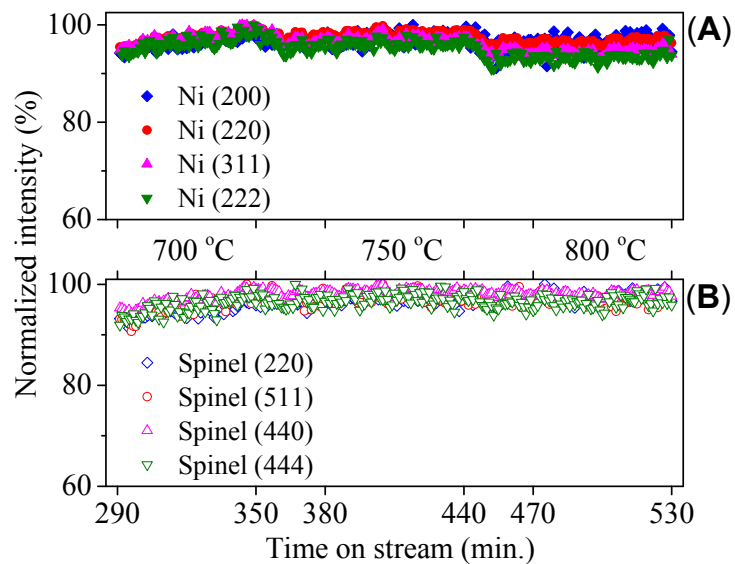


Fig. S2 The normalized intensities of Ni reflections (A), and the spinel support (NiAl_2O_4 and MgAl_2O_4) reflections (B).

Fig. S3 (TEM images)

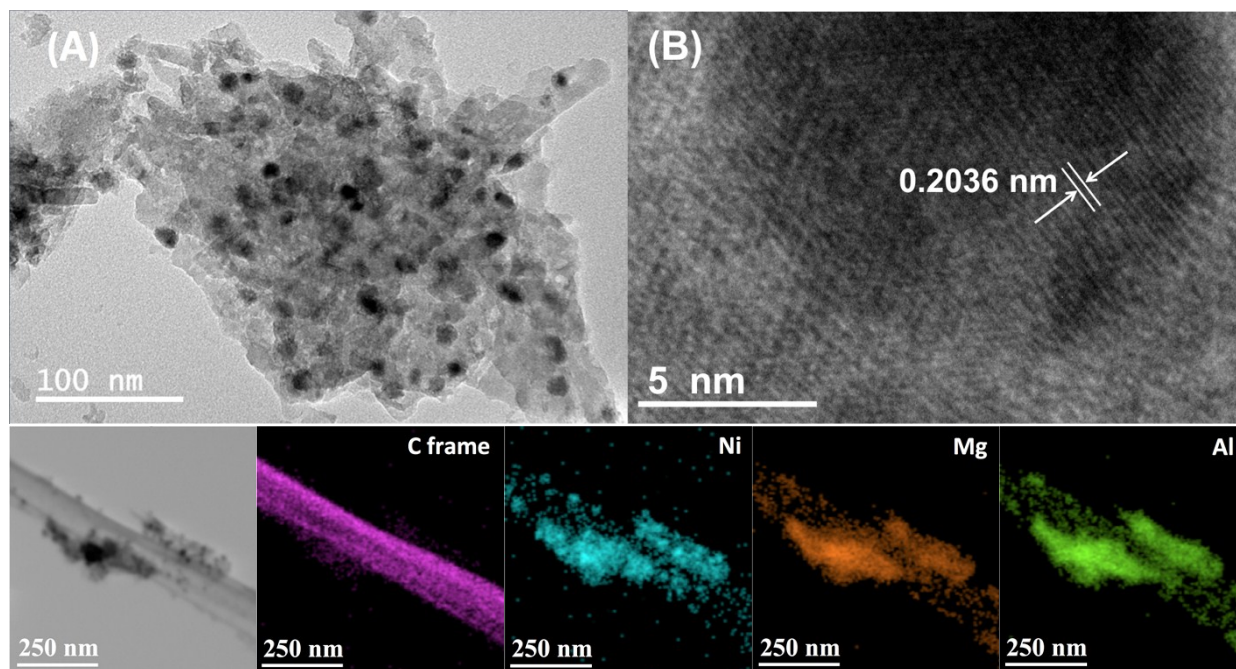


Fig. S3 TEM images (A and B) and EDS mappings (bottom) of NiMgAl catalyst after the entire *in situ* XRD experiment.

Fig. S4 (TGA curve)

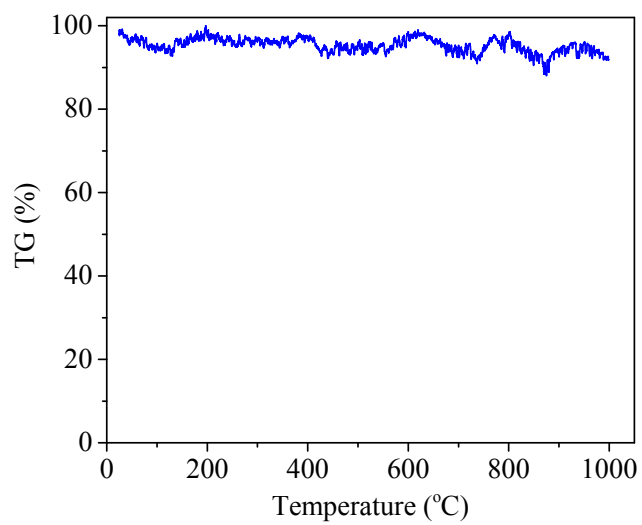


Fig. S4 The TGA curve of NiMgAl catalyst after the entire *in situ* XRD experiment.

Fig. S5 (RGA results)

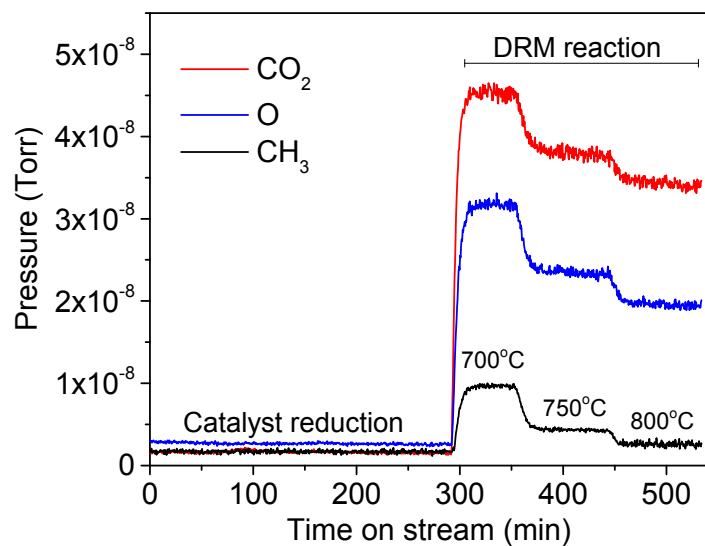


Fig. S5 The mass spectroscopic data of the residual gas plotted with time for the DRM reaction.

Fig. S6 (d-spacing & crystallite size on each reflection)

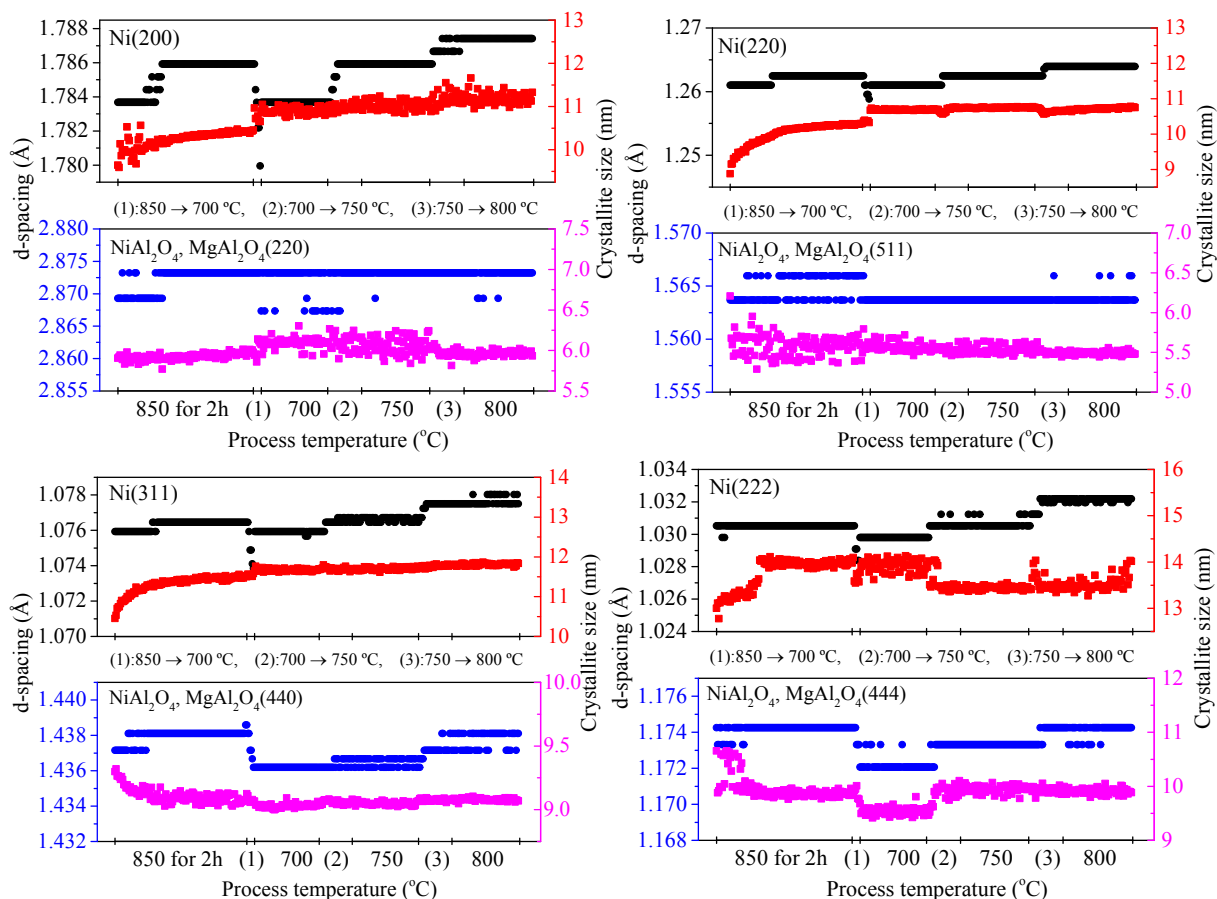


Fig. S6 the crystallite size and d-spacing calculated based on (200), (220), (311) and (222) reflections for Ni phase (top panels), and based on (220), (511), (440) and (444) reflections for NiAl₂O₄ and MgAl₂O₄ (bottom panels).

Fig. S7 (lattice parameter and unit cell volume at reduction and DRM reaction stages)

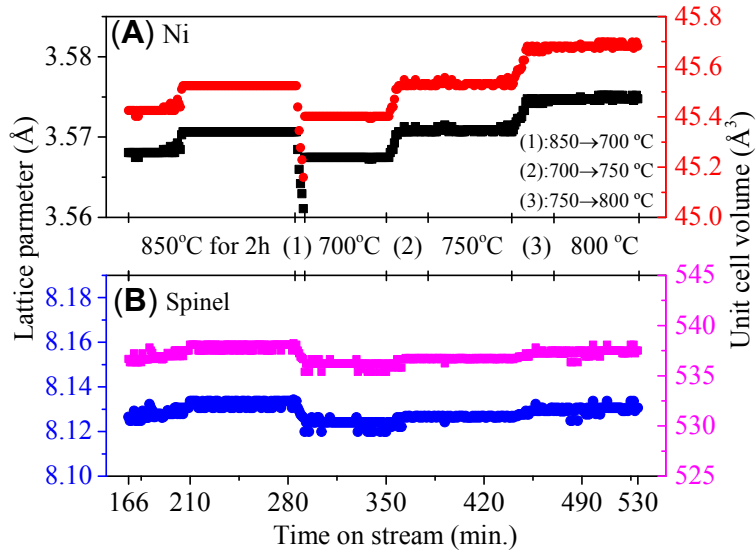


Fig. S7 The average lattice parameter and unit cell volume for the fcc Ni (A) and fcc spinel NiAl_2O_4 and MgAl_2O_4 (B) were calculated based on the d-spacing value and shown the same evolution trend with d-spacing.

For the cubic lattice, the lattice parameter (α) and unit cell volume (V) for any (hkl) reflection are calculated using the following formulas:

$$\alpha_{(hkl)} = d_{(hkl)} \times \sqrt{h^2 + k^2 + l^2}$$

$$V_{(hkl)} = \alpha_{(hkl)}^3$$

Fig. S8 (lattice parameter and unit cell volume at cooling stage)

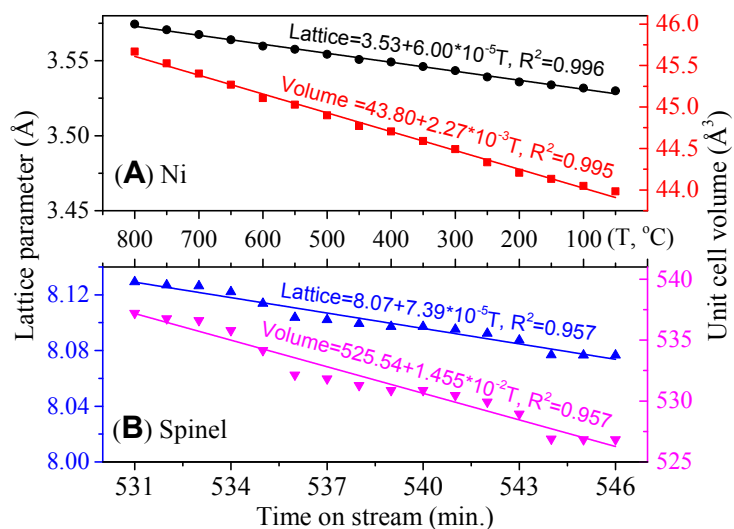


Fig. S8 The average lattice parameter and unit cell volume for the fcc Ni (A) and fcc spinel carrier (B) at the cooling stage after the DRM reaction, which showed the same linear decreasing trend with d-spacing.

For the cubic lattice, the lattice parameter (α) and unit cell volume (V) for any (hkl) reflection are calculated using the following formulas:

$$\alpha_{(hkl)} = d_{(hkl)} \times \sqrt{h^2 + k^2 + l^2}$$

$$V_{(hkl)} = \alpha_{(hkl)}^3$$

Cal. S1 (Determining the composition of NiO_{free}, NiO_{int.} and NiAl₂O₄)

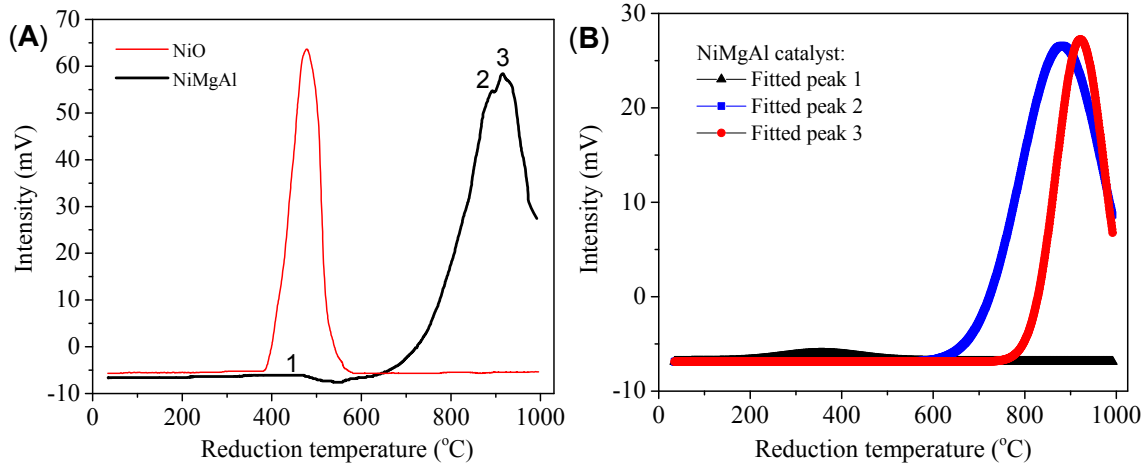


Fig. S9 The TPR profiles of pure NiO sample and NiMgAl catalyst (A), and the separation and integration of peaks 1-3 for NiMgAl catalyst (B).

Table S4 The integration data of peaks 1-3 for NiMgAl catalyst.

NiMgAl catalyst	Ascription	Area (mV·°C)	Height (mV)
Fitted peak 1	NiO _{free}	178.0	0.85
Fitted peak 2	NiO _{int.}	6669.3	33.46
Fitted peak 3	NiAl ₂ O ₄	4051.5	34.12

The data in Table S4 was acquired from Fig. S9B. The area of each species was used to determine its composition.

$$A(\text{Total}) = A(\text{NiO}_{\text{free}}) + A(\text{NiO}_{\text{int.}}) + A(\text{NiAl}_2\text{O}_4) = 178.0 + 6669.3 + 4051.5 = 10898.8$$

$$\%(\text{NiO}_{\text{free}}) = \frac{A(\text{NiO}_{\text{free}})}{A(\text{Total})} = \frac{178.0}{10898.8} \times 100\% = 1.6\%$$

$$\%(\text{NiO}_{\text{int.}}) = \frac{A(\text{NiO}_{\text{int.}})}{A(\text{Total})} = \frac{6669.3}{10898.8} \times 100\% = 61.2\%$$

$$\%(\text{NiAl}_2\text{O}_4) = \frac{A(\text{NiAl}_2\text{O}_4)}{A(\text{Total})} = \frac{4051.5}{10898.8} \times 100\% = 37.2\%$$

Cal. S2 (Determining the effect of temperature on the peak intensity)

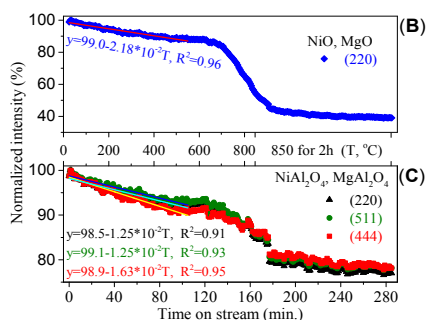


Fig. 2B–C in main manuscript

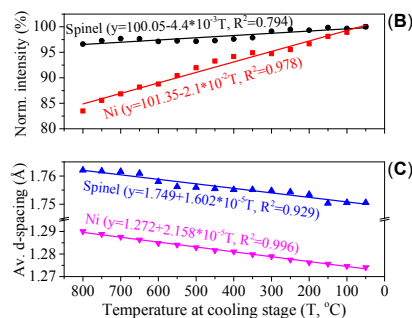


Fig. 4B–C in main manuscript

The intensity of the NiO and NiAl₂O₄ decrease linearly below 550 °C (Fig. 2B–C). However, there is no reduction below 550 °C for NiMgAl catalyst according to the TPR information by ignoring the tiny peak 1 (Fig. S9A). Therefore, this linear decline in XRD intensity before 550 °C was caused by the increase of temperature rather than the reduction of NiO. It is reasonable to make the assumption that the linearity of the temperature effect on the XRD peak intensity can be extended to the entire reduction temperature range, i.e. 850 °C. Since the XRD intensity also linearly changed during the reverse process that the temperature dropped from 800 to 50 °C at the cooling stage after the DRM reaction (Fig. 4B).

The intensity decline caused by the temperature rising during the reduction process for NiO and MgO (220) reflection is:

$$y_{NiO(220), T=850^\circ C} = 99.0 - 0.0218 \times 850 = 80.5$$

$$Intensity_{NiO(220), T=850^\circ C} = 100\% - 80.5\% = 19.5\%$$

The remaining intensities caused by the temperature rising during the reduction process for spinel NiAl₂O₄ and MgAl₂O₄ (220), (511) and (444) reflections are:

$$y_{Spinel(220), T=850^\circ C} = 98.5 - 0.0125 \times 850 = 87.9$$

$$y_{Spinel(511), T=850^\circ C} = 99.1 - 0.0125 \times 850 = 88.5$$

$$y_{Spinel(444), T=850^\circ C} = 98.9 - 0.0163 \times 850 = 85.0$$

Therefore, the intensity drops caused by the temperature raising are:

$$Intensity_{Spinel(220), T=850^\circ C} = 100\% - 87.9\% = 12.1\%$$

$$Intensity_{Spinel(511), T=850^\circ C} = 100\% - 88.5\% = 11.5\%$$

$$Intensity_{Spinel(444), T=850^\circ C} = 100\% - 85.0\% = 15.0\%$$

$$Average Intensity_{Spinel, T=850^\circ C} = \frac{12.1 + 11.5 + 15.0}{3}\% = 12.9\%$$

Cal. S3 (Determining the reduction degree of NiAl₂O₄)

A prerequisite must be addressed that the XRD intensity variation for each phase is proportional to its molar phase change.

We set that there are 100 mol of the NiMgAl catalyst, whose nominal molar composition is $\text{Ni}_{11}\text{Mg}_{20}\text{Al}_{69}$.

Therefore, we get:

$$n(\text{Ni}) = 100 \times 11\% = 11 \text{ mol}$$

$$n(\text{Mg}) = 100 \times 20\% = 20 \text{ mol}$$

$$n(\text{Al}) = 100 \times 69\% = 69 \text{ mol}$$

From the results of TPR peak separation and integration, the molar amount of NiO and NiAl_2O_4 accounts for 62.8% (NiO_{free} 1.6%, NiO_{int} 61.2%), and 37.2%, respectively.

$$n(\text{NiO}) = 11 \times 62.8\% = 6.908 \text{ mol}$$

$$n(\text{NiAl}_2\text{O}_4) = 11 \times 37.2\% = 4.092 \text{ mol}$$

According to the TPR profile, NiO phase can be considered as completely reduced during this reduction process. So, the XRD intensity drop of 61.0% was ascribed to the reduction of NiO and temperature effect. The intensity remaining 39.0% belongs to the MgO phase. We obtain:

$$\frac{n(\text{NiO}) + [\text{Temp.}]}{n(\text{NiO}) + n(\text{MgO}) + [\text{Temp.}]} = 61.0\% \quad \text{or} \quad \frac{n(\text{MgO})}{n(\text{NiO}) + n(\text{MgO}) + [\text{Temp.}]} = 39.0\% \quad (\text{A})$$

$$\frac{[\text{Temp.}]}{n(\text{NiO}) + n(\text{MgO}) + [\text{Temp.}]} = 19.5\% \quad (\text{B})$$

Combine (A) and (B), we get:

$$n(\text{MgO}) = \frac{39\% \times n(\text{NiO})}{100\% - 19.5\% - 39\%} = \frac{39\% \times 6.908}{41.5\%} = 6.492 \text{ mol}$$

$$n(\text{MgAl}_2\text{O}_4) = n(\text{Mg}) - n(\text{MgO}) = 20 - 6.492 = 13.508 \text{ mol}$$

The intensity decline of 22.2% for NiAl_2O_4 and MgAl_2O_4 was caused by the reduction of NiAl_2O_4 and temperature rise:

$$\frac{n(\text{NiAl}_2\text{O}_{4_reduced}) + [\text{Temp.}]}{n(\text{NiAl}_2\text{O}_4) + n(\text{MgAl}_2\text{O}_4) + [\text{Temp.}]} = 22.2\% \quad (\text{C})$$

$$\frac{[\text{Temp.}]}{n(\text{NiAl}_2\text{O}_4) + n(\text{MgAl}_2\text{O}_4) + [\text{Temp.}]} = 12.9\% \quad (\text{D})$$

Combining (C) and (D), we obtain the following:

$$n(\text{NiAl}_2\text{O}_{4_reduced}) = \frac{(22.2\% - 12.9\%) \times [n(\text{NiAl}_2\text{O}_4) + n(\text{MgAl}_2\text{O}_4)]}{(100\% - 12.9\%)} = \frac{0.093 \times [4.092 + 13.508]}{0.871} = 1.879 \text{ mol}$$

$$(\text{NiAl}_2\text{O}_4)_{\text{reduction degree}} = \frac{n(\text{NiAl}_2\text{O}_{4_reduced})}{n(\text{NiAl}_2\text{O}_4)} \times 100\% = \frac{1.879}{4.092} \times 100\% = 45.9\%$$

Cal. S4 (Determining the phase compositions of fresh and reduced catalysts)

Based on the calculation from Cal. S3, we know that:

$$n(\text{NiO}) = 6.908 \text{ mol}$$

$$n(\text{MgO}) = 6.492 \text{ mol}$$

$$n(\text{NiAl}_2\text{O}_4) = 4.092 \text{ mol}$$

$$n(\text{MgAl}_2\text{O}_4) = 13.508 \text{ mol}$$

$$n(\text{Al}_2\text{O}_3) = \frac{n(\text{Al}) - n(\text{NiAl}_2\text{O}_4) \times 2 - n(\text{MgAl}_2\text{O}_4) \times 2}{2} = \frac{69 - 4.092 \times 2 - 13.508 \times 2}{2} = 16.9 \text{ mol}$$

Therefore, the phase composition for the **fresh catalyst** sample is:

$$\begin{aligned} n(\text{Total}_{\text{fresh}}) &= n(\text{NiO}) + n(\text{MgO}) + n(\text{Al}_2\text{O}_3) + n(\text{NiAl}_2\text{O}_4) + n(\text{MgAl}_2\text{O}_4) = 6.908 + 6.492 + 16.9 \\ &+ 4.092 + 13.508 = 47.9 \text{ mol} \end{aligned}$$

$$\%(\text{NiO}) = \frac{n(\text{NiO})}{n(\text{Total}_{\text{fresh}})} = \frac{6.908}{47.9} \times 100\% = 14.4\%$$

$$\%(\text{MgO}) = \frac{n(\text{MgO})}{n(\text{Total}_{\text{fresh}})} = \frac{6.492}{47.9} \times 100\% = 13.6\%$$

$$\%(\text{Al}_2\text{O}_3) = \frac{n(\text{Al}_2\text{O}_3)}{n(\text{Total}_{\text{fresh}})} = \frac{16.9}{47.9} \times 100\% = 35.3\%$$

$$\%(\text{NiAl}_2\text{O}_4) = \frac{n(\text{NiAl}_2\text{O}_4)}{n(\text{Total}_{\text{fresh}})} = \frac{4.092}{47.9} \times 100\% = 8.5\%$$

$$\%(\text{MgAl}_2\text{O}_4) = \frac{n(\text{MgAl}_2\text{O}_4)}{n(\text{Total}_{\text{fresh}})} = \frac{13.508}{47.9} \times 100\% = 28.2\%$$

After reduction, the NiAl_2O_4 was reduced to Ni and Al_2O_3 , therefore:

$$n(\text{NiAl}_2\text{O}_4)_{\text{reduced}} = 1.879 \text{ mol}$$

$$n(\text{Ni}) = n(\text{NiO}) + n(\text{NiAl}_2\text{O}_4)_{\text{reduced}} = 6.908 + 1.879 = 8.787 \text{ mol}$$

$$n(\text{NiAl}_2\text{O}_4)_{\text{after red.}} = n(\text{NiAl}_2\text{O}_4) - n(\text{NiAl}_2\text{O}_4)_{\text{reduced}} = 4.092 - 1.879 = 2.213 \text{ mol}$$

$$n(\text{Al}_2\text{O}_3)_{\text{after red.}} = n(\text{Al}_2\text{O}_3) + n(\text{NiAl}_2\text{O}_4)_{\text{reduced}} = 16.9 + 1.879 = 19.113 \text{ mol}$$

$$n(\text{MgO})_{\text{after red.}} = n(\text{MgO}) = 6.492 \text{ mol}$$

$$n(\text{MgAl}_2\text{O}_4)_{\text{after red.}} = n(\text{MgAl}_2\text{O}_4) = 13.508 \text{ mol}$$

So, the phase composition for the reduced catalyst sample is:

$$\begin{aligned} n(\text{Total}_{\text{after red.}}) &= n(\text{Ni}) + n(\text{MgO})_{\text{after red.}} + n(\text{Al}_2\text{O}_3)_{\text{after red.}} + n(\text{NiAl}_2\text{O}_4)_{\text{after red.}} + n(\text{MgAl}_2\text{O}_4)_{\text{after red.}} = \\ &8.787 + 6.492 + 19.113 + 2.213 + 13.508 = 50.113 \text{ mol} \end{aligned}$$

$$\%(\text{Ni}) = \frac{n(\text{Ni})}{n(\text{Total}_{\text{after red.}})} = \frac{8.787}{50.113} \times 100\% = 17.5\%$$

$$\%(MgO)_{after\ red.} = \frac{n(MgO)}{n(Total_{after\ red.})} = \frac{6.492}{50.113} \times 100\% = 13.0\%$$

$$\%(Al_2O_3)_{after\ red.} = \frac{n(Al_2O_3)_{after\ red.}}{n(Total_{after\ red.})} = \frac{19.113}{50.113} \times 100\% = 38.1\%$$

$$\%(NiAl_2O_4)_{after\ red.} = \frac{n(NiAl_2O_4)_{after\ red.}}{n(Total_{after\ red.})} = \frac{2.213}{50.113} \times 100\% = 4.4\%$$

$$\%(MgAl_2O_4)_{after\ red.} = \frac{n(MgAl_2O_4)}{n(Total_{after\ red.})} = \frac{13.508}{50.113} \times 100\% = 27.0\%$$

Reference

- 1 Z. Bao, Y. Lu, J. Han, Y. Li and F. Yu, *Appl. Catal. A: Gen.*, 2015, **491**, 116–126.
- 2 T. R. Jensen, T. K. Nielsen, Y. Filinchuk, J.-E. Jorgensen, Y. Cerenius, E. M. Gray and C. J. Webb, *J. Appl. Crystallogr.*, 2010, **43**, 1456–1463.
- 3 D. P. Shoemaker, Y. J. Hu, D. Y. Chung, G. J. Halder, P. J. Chupas, L. Soderholm, J. F. Mitchell and M. G. Kanatzidis, *Proc. Natl. Acad. Sci.*, 2014, **111**, 10922–10927.
- 4 W. Xu, Z. Liu, A. C. Johnston-Peck, S. D. Senanayake, G. Zhou, D. Stacchiola, E. A. Stach and J. A. Rodriguez, *ACS Catal.*, 2013, **3**, 975–984.
- 5 B. P. Dhonge, T. Mathews, S. T. Sundari, C. Thinaharan, M. Kamruddin, S. Dash and A. K. Tyagi, *Appl. Surf. Sci.*, 2011, **258**, 1091–1096.
- 6 B. Sathyaseelan, I. Baskaran and K. Sivakumar, *SNL*, 2013, **03**, 69–74.
- 7 T. Shiono, K. Shiono, K. Miyamoto and G. Pezzotti, *J. Am. Ceram. Soc.*, 2000, **83**, 235–37.
- 8 P. J. Chupas, K. W. Chapman, C. Kurtz, J. C. Hanson, P. L. Lee and C. P. Grey, *J. Appl. Cryst.*, 2008, 822–824.